Available online at www.giornaleitalianoendodonzia.it

ORIGINAL ARTICLE

# Application of artificial intelligence in a visual-based fluid motion estimator surrounding a vibrating EDDY® tip


## ABSTRACT

***Aim:*** *To improve our initial understanding of the vibrational behavior and fluid flow of an EDDY® tip when irrigation is activated using artificial intelligence (AI).*
***Methodology:*** *A straight glass model was filled with a solution containing 3% NaOCl. A-28 mm polymer noncutting #20 0.04 taper file was driven by an air sonic handpiece at 6,200 Hz for five seconds. The fluid flow behavior was visualized using a Miro 320S high-speed imaging system (Phantom, Wayne, NJ, USA). The recordings of the hydrodynamic response were then analyzed using motion estimation program, supported by LiteFlowNet.*
***Results:*** *Rapid fluid flow was visualized clearly in the model when activated by an air sonic driven EDDY® tip. The distal end of the EDDY® tip generated a near-wall high-gradient velocity apically in all directions of the oscillation.*
***Conclusions:*** *The proposed motion estimation program, supported by LiteFlowNet, could perform flow estimation of a non-PIV experiment in detail.*



**Harry Huiz Peeters**[1*]
**Faber Silitonga**[2]
**Lavi Zuhal**[2]

[1]*Laser Research Center in Dentistry, Bandung, Indonesia*

[2]*Faculty of Mechanical and Aerospace Engineering, Bandung Institute Technology, Bandung, West Java, Indonesia*



*Received 2021, December 17*
*Accepted 2022, January 24*

**KEYWORDS** *artificial intelligence, EDDY® tip, endodontics, natural frequency, shear stress*



**Corresponding Author**
Harry Huiz Peeters | Cihampelas 41 Bandung Jawa Barat | Indonesia
Tel +620224236007 Fax: +620226127540 | Email: h2huiz@cbn.net.id



Peer review under responsibility of Società Italiana di Endodonzia
10.32067/GIE.2021.35.02.50

## Introduction

A new polyamide tip, referred to as an EDDY® tip (VDW, Munich, Germany), has recently been developed for activating root canal irrigants and released onto the market. An EDDY® tip is a smooth polymer tip driven by an air sonic scaler at 5,100-6,200 Hz. Numerous studies have found sonically and ultrasonically driven electrical devices to be effective in cleaning root canals (1-5). Several researchers have found that sonically activated irrigation is less effective than its ultrasonically activated counterpart, while others have suggested that the two methods produce comparable results (6-8). However, the physical mechanism relating to the efficiency of EDDY® tip has yet to be assessed.

Several studies on dentistry have employed powerful particle image velocimetry (PIV) technology to observe the natural flow behavior of hydrodynamic response during irrigation activation (9-12). This conventional PIV method uses microscopic tracer particles intended to be a non-intrusive means of obtaining a deeper insight into complex flow phenomena used in the measuring of a velocity field. The tracer particles previously seeded into the flow medium do not affect the natural flow motion. The displacement of the seeding particles is recorded by means of a high-speed digital imaging system and subsequently analyzed using a specific program such as cross-correlation with a window deformation iterative method to identify the velocity distribution in the investigated location (13-15).

At the present time, in order to further improve the PIV image-processing program, the implementation of a state-of-the-art innovation constitutes a potential solution. A deep learning approach for motion estimation has shown promising results with higher accuracy and enhanced computational performance (16). Currently, the LiteFlowNet network, a state-of-the-art deep learning model used for motion estimation, has been developed by Hui and colleagues (17). The program utilizes a relatively smaller model size than the other solutions, thus enabling faster inference speed. Furthermore, reproducing a deep learning model from estimator programs is not significantly different to undertaking measured investigations using PIV image processing method. The differences occur only in cases of different randomization incorporating floating number error (18). In dentistry, an artificial intelligence application model has been employed to support the clinical decision-making process in certain clinical disciplines (19) such as radiology (20-22), endodontics (23), and surgery (24).

The main challenge of this study is to develop a deep learning estimator for non-PIV (absence of seeding particles) based on LiteFlowNet (17) which can be applied to a relatively limited area such as a root canal space as a means of producing high-resolution images. Furthermore, the program can process a non-particle image pair input to produce a velocity field output with displacement vectors at every pixel.

To the best of our knowledge, no previous studies of velocity field estimation of hydrodynamic response in a small area relating to air sonic driven EDDY® tips during activation of an irrigation solution using a deep learning program have been conducted. In the present non-PIV study, the occurring phenomena were investigated by acquiring real-time data using a transparent glass block model of a root canal in order to visualize its behavior when in the solution.

## Materials and Methods

*Basic visualization*

The study was designed to observe the hydrodynamic response to EDDY® tip solution activation in the root canal model. The process was recorded using a Phantom Miro 320S high-speed digital imaging system (Wayne, NJ, USA) which incorporated a macro lens capable of producing 25,000 frames per second with 320×240 pixels per image (60 mm, f/2.8; Nikon, Tokyo, Japan). Each sample was illuminated by means of a Fibre-Lite LMI-6000 LED continuous light source (Dolan-Jenner In-

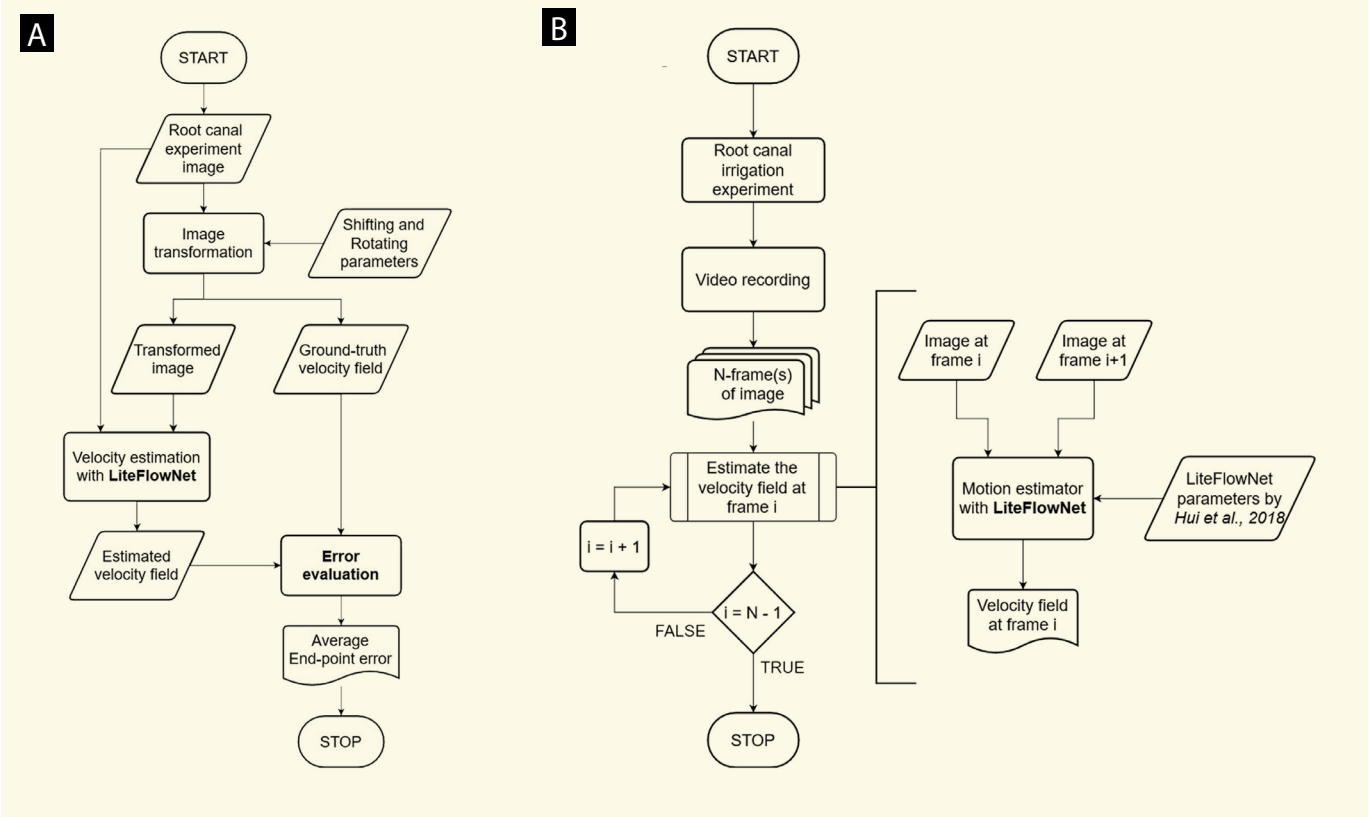


**Figure 1**
**A)** The deep learning motion estimator process in an optically accessible root canal model. **B)** The workflow featured in each validation test.

dustries, Boxborough, MA, USA). The study method implemented was designed in such a manner as to be non-destructive. A single glass tooth model was used during each treatment to ensure uniformity of root canal width and size. After each test, the model was carefully cleaned for re-use in the subsequent one. Experiments were conducted three times on each sample. In order to obtain estimation quantitative data images, the recordings of the hydrodynamic response were analyzed using an in-house PIV software developed by the Aerodynamics Laboratory at ITB (Institut Teknologi Bandung, West Java, Indonesia). This software utilizes optical flow with a convolutional neural network for velocity field estimation rather than measured experimental PIV settings with tracer particles.

*Sonic parameters and procedure*
A-28 mm polymer noncutting # 20/0.04 (VDW) tip was screwed onto a Ti-Max S970 air scaler (NSK, Tochigi, Japan) set at level 3 (5,800–6,200 Hz) in accordance with the manufacturer's instructions and employed to activate the irrigant. The sample was subjected to active sonic irrigation without use of a water spray, while the tip was activated passively without any filing motion.

*Experiment: visualization of an EDDY® tip during irrigant activation*
The conditions within a straight root canal were simulated and visualized using a glass block model with an artificial canal and pulp cavity acting as a reservoir (Kimia Farma, Bandung, West Java, Indonesia). The crown height was one of 7 mm, while the root length was 18 mm with an inner diameter of 0.4 mm at the apex and 0.06 taper. Each model was filled with a solution containing 3% NaOCl. The apex of the model was sealed with composite to simulate the internal conditions of a root canal. The sonic instrument tip was inserted to a depth of 3 mm below the orifice and activated passively for five seconds without any filing motion. Maintenance of the desired position, fluid activation and pre-

vention of the tip binding vibrating against the canal wall were ensured by fixing the tip in a holder.

*Image processing*

Data from non-PIV experiments was extracted by means of a deep learning estimator incorporating a deep learning estimator incorporating PIV software developed by the Aerodynamics Laboratory at ITB (Institut Teknologi Bandung, West Java, Indonesia). Since the images obtained during the conduct of this experiment were not of PIV particles, the non-enhanced LiteFlowNet version (17) proved more suitable. This was due to the LiteFlowNet model being trained using images with general objects (and RGB colored), unlike the PIV-LiteFlowNet-en that is trained specifically with grayscale particle images. It is important to note that the same program was employed in this case by reproducing the PIV-LiteFlowNet-en in a Python program with PyTorch, thereby allowing the user to control the modification of each layer. Therefore, in order to generate a LiteFlowNet version, the user should disregard the last NetE level and impose the LiteFlowNet trained weights. The flowchart outlining the stages of the data execution process is contained in Figure 1A.

*Program validation*

It is necessary to prove the validity of the motion program in handling the images resulting from the root canal experiment with LiteFlowNet. Thus, a validation test was performed by transforming several images in order to estimate the velocity field produced by the corresponding transformation. Figure 1B presents the test procedure relating to a single sample image. To validate the images generated during the experiment, they were either shifted or rotated according to their respective randomized input parameters. Therefore, it also proved possible to extrapolate the ground-truth velocity field from the parameters. The LiteFlowNet estimated the velocity field occurring between the original and transformed images. The average end-point error (AEE) was calculated on the basis of the estimated and ground-truth velocity fields. The experiment images were shifted randomly between -11 to 11 pixels in both vertical and horizontal directions. These parameters were selected on the basis of a study conducted by Butler et al. (25) that a displacement above 12 ppf is considered to be significant. This resulted in various shifting combinations, ranging from displacement of 0.5 pixel per frame (ppf) to one of 14.7 ppf. Evaluation based on different velocity gradients and rotational transformation was also included. The images were then rotated randomly from -18 to 18 degree direction,

In order to avoid potential confusion due to the blank pixel, error evaluation was performed only around the center region of the images, as depicted by the red- bordered boxes contained in Figure 2. While avoiding the blank pixels, the evaluation region relating to the shifting transformation, Figure 2B captured the most crucial area located around the irrigation solution. On the other hand, the smaller bordered box for the rotational test shown in Figure 2E was intended to allow larger image rotation of up to 18 degrees while maintaining reasonable pixel displacement. Hence, error evaluation of high-velocity gradient cases is facilitated by the larger image rotation. The greatest recorded pixel displacement during the rotational test was one of 14.1 ppf. The evaluation results for both the shifting and rotational transformation tests are presented in Table 1.

The 99$^{th}$ percentile AEE value is also provided to enable analysis of the critical condition. The rotational test indicated that

**Table 1**
**Average end-point error evaluation (AEE) for both shifting and rotational transformation. The mean value and the 99th percentile errors are presented for both tests**

| Method | AEE |
|---|---|
| MPI Sintel - final | 5.38 |
| KITTI12 | 1.60 |
| Shifting test - mean | 0.10 |
| Shifting test - 99th | 0.26 |
| Rotation test - mean | 0.22 |
| Rotation test - 99th | 1.31 |

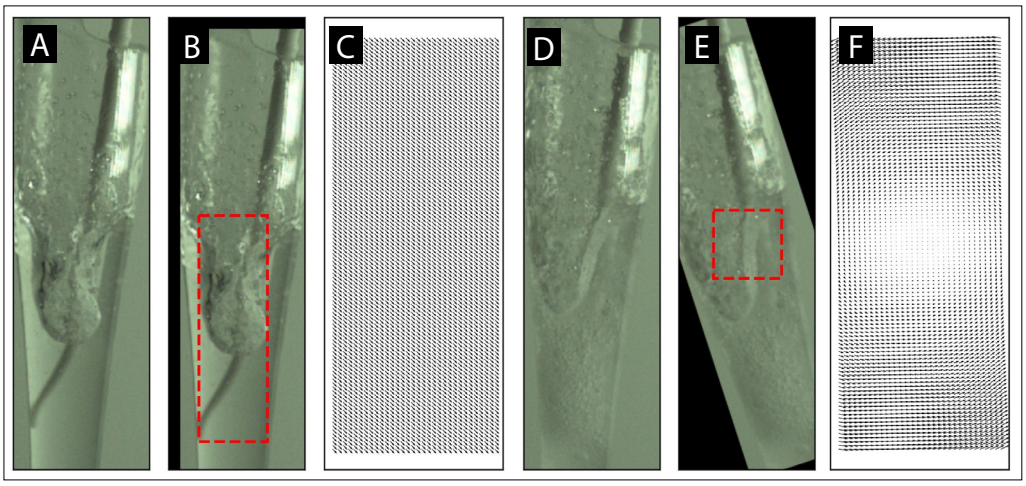


**Figure 2**
Illustration of the original and transformed. **A)** Sample experiment image #1, **B)** image #1 shifted using a translational velocity field, **C)**, the quiver graph of translational velocity field on each pixel. **D)** Sample experiment image #2, **E)** image #2 rotated using rotational velocity field, and **F)** the quiver graph of rotational velocity field on each pixel. dense velocity fields within small-scale flow structures near the wall were visualized.

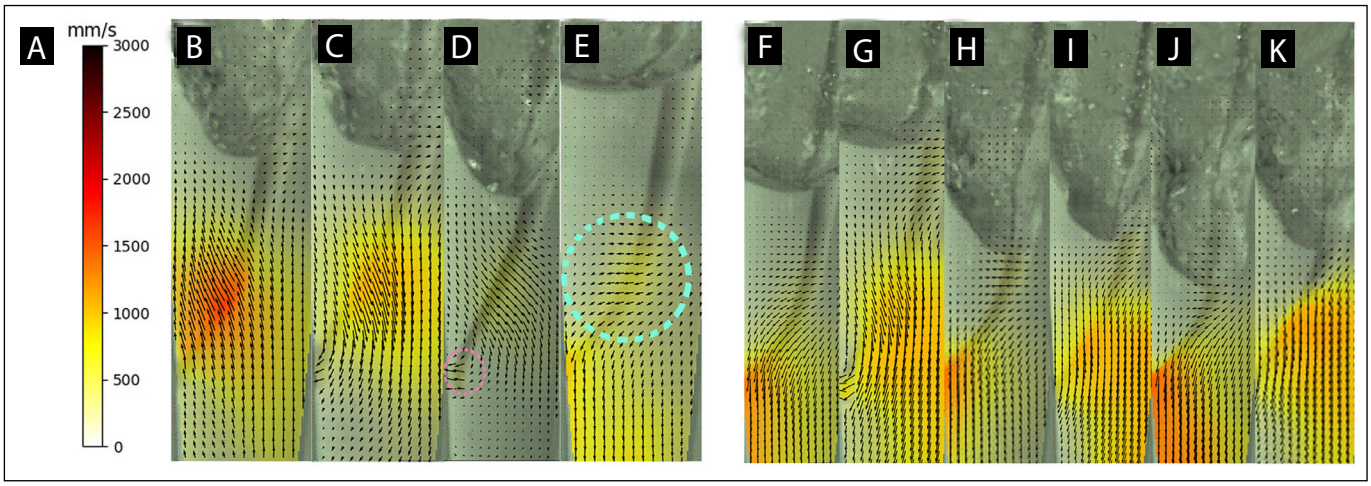


**Figure 3**
**A)** The velocity scale for each image is indicated by the color bar on the left. Direction of the flow caused by an EDDY® oscilating tip (indicated by solid arrows). **B)** Upward direction; **C)** downward direction; **D, E)** the broken circles indicate the flow pattern occasionally occuring perpendicular to the axial of the tip. **F-K)** Indicating instantaneous dense velocity fields within small-scale flow structures near the wall were visualized. The orange to red color indicates the location where a near-wall high-velocity gradient occurs.

the highest 1% AEE results were all produced by those images rotated by >16.6 degree. It was suspected that the higher velocity gradient (due to greater image rotation) constituted the main causal factor. This was due to there being a strong positive correlation between the image rotation angle that was proportional to the velocity gradient and the AEE with a Pearson's correlation coefficient (PCC) score of 0.64. On the other hand, the shifting test proved that there was almost no correlation between the pixel displacement and the AEE score of -0.06 PCC. This is reason for the highest 1% AEE results of the shifting test being produced by images transformed with varying displacement ranging from 0.55 ppf to 14.7 ppf. Therefore, it can be concluded that the effect of larger pixel displacement was insignificant to the high-velocity gradient in terms of reducing the program performance. Furthermore, the tests showed that the LiteFlowNet-based estimator program was valid for processing the root canal experiment images. It is because all of the AEE results were relatively lower than those of the LiteFlowNet benchmark (17) in the popular dataset (MPI Sintel and KITTI) (25, 26), even for the 99$^{th}$ percentile value.

## Results

*Data extraction*

The study results indicate that the modified non-enhanced LiteFlowNet program successfully extracted non-particle image pair input, producing velocity field output with displacement vectors in every pixel. Furthermore, the program provided detailed high-resolution images enabling smaller scale motion detection, while also gener-

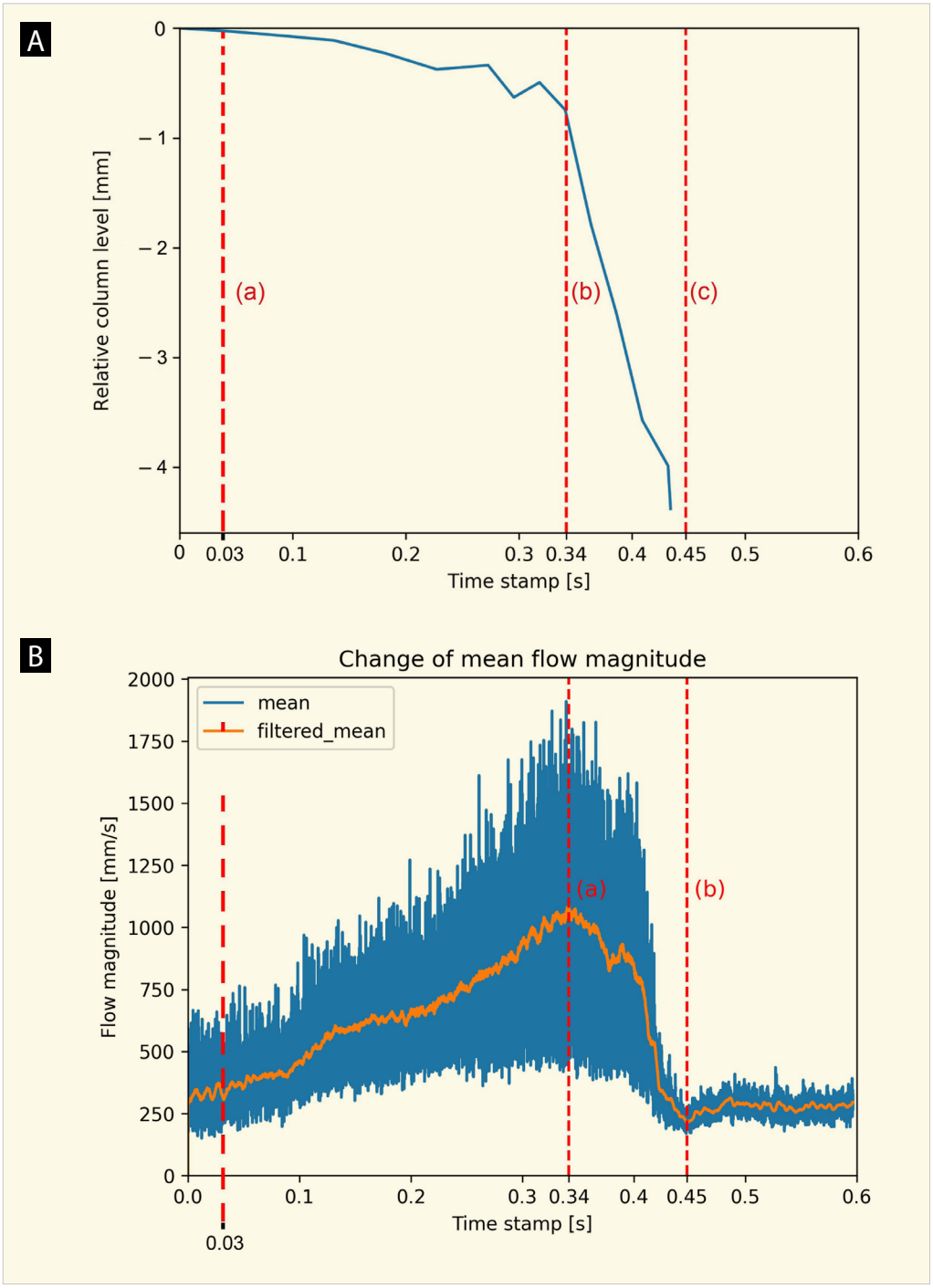


**Figure 4**
**A)** Column level of air depression and **B)** Average flow magnitude.

ating a dense motion field for all images, and rapidly completing computer processing.

*Experiment*

The flow motion was highly unsteady. In order to highlight the observation, the study focused on only a limited portion of the canal to enable velocity field visualization. The portion was located around the distal end of the tip. The instantaneous images contained in Figure 3 illustrate the flow pattern of the solution near the distal end of the tip where the highest amplitude

occurs. The flow pattern of strong axial components was both upwards and downwards (figure 3B and C). A flow pattern perpendicular to the axial flow along the canal was periodically observed (figure 3D and E). A periodic flow pattern within which velocity gradients occurred near the wall during activation, such as shown in Figure 3F-K, was observed. The velocity fields within this region (shown in red) were approximately three times higher than those in the surrounding area. The length of the arrows also indicates the magnitude of the velocity.
Figure 4 depicts the duration of energy accumulation and the average fluid magnitude during activation. The correlation between air column depression and bubbles formation during activation could be observed.

## Discussion

The experiment results revealed that the process of EDDY® tip activation in the root canal model occurred in three stages.
**Stage 1:** the vibrating EDDY® tip transferred its energy to the solution and created waves which, in turn, caused surface waves to form at the interfaces. In the air-solution interface system, the surface of the solution moved downwards on one side and upwards on the other. The duration of this energy accumulation period was in the range of the initial 0-0.03 seconds (figure 4Aa).
**Stage 2:** this stage lasted between approximately 0.03 and 0.34 seconds (figure 4Aa-b). When the amplitude reached or approached its peak, kinetic energy increased to the point that it was sufficiently high to disrupt the interface with an average fluid magnitude close to 300 mm/sec. This disruption, in turn, forced part of the solution upwards into the coronal portion where droplets formed on the wall. Their accumulation caused mass displacement of the solution, while downward pressure waves subsequently forced the air to displace it. The solution and the air moved spontaneously and simultaneously. The pressure of the air on the solution forced it far beyond the interface which created an air depression column. The possible reasons for this may be that the specific natural frequency of the EDDY® tip was achieved, while the amplitude concomitantly approached or reached its peak. It means that, at the setting concerned, one of the natural frequencies of the tip matched the frequency of excitation.
By way of confirmation, the results of the pilot study conducted demonstrated that when an Eddy tip was being forced to vibrate in the air at its natural frequency for less than a second the distal end of the tip might separate. This means that the EDDY® tip achieved its resonant frequency which caused damage due to excessive vibration (27). The velocity of the moving air depression column was approximately 20 mm/sec. During this period, accumulation of energy occurred in the form of flow magnitude generating velocity field throughout the canal. Significant data at this stage indicates that the natural frequency of the tip generates intense solution flow. It was observed that the flow pattern periodically moved up and down throughout the canal (figure 3B, 3C). This action may develop a push-pull mechanism by which removal of smear layer and debris will be enhanced. Furthermore, the natural frequency of the tip produces a near-wall high-velocity gradient which is proportional to wall-shear stresses. The areas of significant changes in velocity over a short distance are indicated in red (figure 3 F-K). From a fluid dynamic perspective, a near-wall high-velocity gradient and the bulk transports of solution are, potentially, the most important variables of the cleaning process within the root canal during activation (11). Finally, it was observed that high-velocity gradient on the wall largely occurred more apically (around the lower end of the tip) and periodically in the same area as indicated in red (figure 3 F-K). The shear stress coverage area was approximately 3-4 mm which enhances the efficacy of the cleaning effect around the apex.
Based on the data relating to this stage, it is recommended that the tip should be moved up and down in order to distribute the shear stresses evenly along the canal, while the pumping action of the tip induc-

es additional shear stresses on the wall. Its cleaning efficacy has been attributed to the combination of either mechanical forces or fluid dynamics with chemical irrigants (28-30). Indeed, this stage is a crucial one within which the near-wall high-velocity gradients are of approximately 0.30 seconds in duration. Within clinical settings, it would be possible for irrigant activation with the cleaning process relating to the entire single root canal to be completed within 30 seconds, thereby reducing treatment time. Additional studies are required to produce further confirmatory evidence in support of this assumption.

**Stage 3:** during the first 350,000-430,000 µs, the oscillating free end of the EDDY® tip (antinode) did not generate bubbles. After approximately 450,000 µs (figure 4Ab-c), the air depression column reached the distal end of the tip (antinode) where the maximum flow velocity reached approximately 1,500 mm/sec, as indicated by the red section of the color bar (figure 3A). Intense bubble fragmentation occurred when the bubbles reached the oscillating distal end of the tip. The vibrations of the free end of the tip generated new bubbles, a continuous process (340,000-450,000 µs) occurring during activation which culminated in the entire canal being filled largely with micro-bubbles (i.e., clouds of bubbles), while simultaneously producing circular solution flow along the root canal wall and creating a chaotic pattern at 450,000 µs. The results showed that the bubble cloud at the distal end of the tip was formed at around 450,000 µs post- EDDY® tip activation. The life cycle of an observed bubble 500 µm in diameter ranges from 300,000 to 500,000 µs. This intense bubble formation can cause an expansion in volume of up to 1,600 times the original, thereby enabling easier access of the irrigant to the apical region of the canal which might assist in the cleaning ability of various shapes (31). This bubble formation was visualized by means of high-speed imaging. However, during intense bubble formation, when the velocity fields in the solution could not be observed simultaneously, the velocity decreased to its lowest level reaching a constant speed of approximately 250 mm/sec (figure 4B, C) where near-wall velocity gradients did not occur. As a consequence of this phenomenon, continuous replenishment of irrigation solution during activation is recommended as this may reduce the prolonged bubble regime.

Interestingly, the modified estimator program appears to offer the considerable advantage of high efficiency through a reduction in time image processing compared to the original PIV program (32). The whole image extracting process (approximately 13,000 images) employed in this study was of approximately an hour in duration. Furthermore, the study did not require a complicated experimental set-up but one which was, ultimately, extremely cost effective.

## Conclusions

The results indicate that the proposed LiteFlowNet-supported motion estimation program was able to conduct detailed flow estimation of a non-PIV experiment and extract dense velocity fields. Moreover, it was capable of capturing transient flow behavior, a near-wall high-velocity gradient and intense bubble formation occurring in a restricted area when the solution was activated by an air sonic driven EDDY® tip. More importantly, there is enormous potential for the development of related topics and this model facilitates further similar research in dentistry.

## Clinical Relevance

Detailed flow pattern during irrigant activation is a fundamental information. Clinicians may use this information to modify treatment procedures to achieve better expected results.

## Conflict of Interest

The authors declare that no conflicts of interests exist regarding the contents of this article.

## Acknowledgement

The authors would like to express their gratitude to Professor Zainal Abidin Ph.D

of Institut Teknologi Bandung (Bandung, Indonesia), Mr. Wowo Watumas of the Phantom Company and Ms. Elvira Theola Judith of the Faculty of Dentistry, Universitas Maranatha (Bandung, Indonesia) for their constructive and supportive contributions to discussions regarding the contents of this article.

## References

1 *Martin H. Ultrasonic disinfection of the root canal. Oral Surg Oral Med Oral Pathol Oral Radiol 1976;42:92-9.*
2 *Cunningham WT, Martin H. A scanning electron microscope evaluation of root canal debridement with the endosonic ultrasonic synergistic system. Oral Surg Oral Med Oral Pathol Oral Radiol 1982;53:527-31.*
3 *Cunningham WT, Martin H, Forrest WR. Evaluation of root canal debridement by the endosonic ultrasonic synergistic system. Oral Surg Oral Med Oral Pathol Oral Radiol 1982;53:401-4.*
4 *Sabins RA, Johnson JD, Hellstein JW. A comparison of the cleaning efficacy of short-term sonic and ultrasonic passive irrigation after hand instrumentation in molar root canals. J Endod 2003;29:674-8.*
5 *Lee SJ, Wu MK, Wesselink PR. The effectiveness of syringe irrigation and ultrasonics to remove debris from simulated irregularities within prepared root canal walls. Int Endod J 2004;37:672-8.*
6 *Jensen SA, Walker TL, Hutter JW, Nicoll BK. Comparison of the cleaning efficacy of passive sonic activation and passive ultrasonic activation after hand instrumentation in molar root canals. J Endod 1999;25:735-8.*
7 *Plotino G, Grande NM, Mercade M, et al. Efficacy of sonic and ultrasonic irrigation devices in the removal of debris from canal irregularities in artificial root canals. J Appl Oral Sci 2019;27:1-6.*
8 *Gambarini G, Miccoli G, Di Carlo S, Iannarilli G, Lauria G, Di Nardo D, Seracchiani M, Khrenova T, Bossù M, Testarelli L. Sonic vs Ultrasonic activation of sodium hypoclorite for root canal treatments. In vitro assessment of debris removal from main and lateral canals. G Ital Endod 2020;34:90-6.*
9 *Jiang LM, Verhaagen B, Versluis M, van der Sluis LW. Evaluation of a sonic device designed to activate irrigant in the root canal. J Endod 2010;36:143-6.*
10 *Koch JD, Smith NA, Garces D, Gao L, Olsen FK. In Vitro Particle Image Velocity Measurements in a Model Root Canal: Flow around a Polymer Rotary Finishing File. J Endod 2014;40:412-6.*
11 *Koch JD, Jaramillo DE, DiVito E, Peters OA. Irrigant flow during photon-induced photoacoustic streaming (PIPS) using Particle Image Velocimetry (PIV). Clin Oral Investig 2016;20:381-6.*
12 *Robinson JP, Macedo RG, Verhaagen B, et al. Cleaning lateral morphological features of the root canal: the role of streaming and cavitation. Int Endod J 2018;51:e55–e64.*
13 *Raffel M, Willert C, Kompenhans J. Particle image velocimetry: a practical guide. 1st edn Berlin, Heidelberg: Springer,1998.*
14 *Stepen. Development, Evaluation and Application of Image Processing Code for Digital Particle Image Velocimetry (DPIV) (MA Thesis) (2011). Bandung, Indonesia: Institut Teknologi Bandung. https://digilib.itb.ac.id/index.php/gdl/view/17303.*
15 *Octavianus, F. Development of Multi-Processing Python-based Stereoscopic Digital Particle Image Velocimetry. (Bachelor's Thesis) (2018). Bandung, Indonesia: Institut Teknologi Bandung.*
16 *Cun YL, Matan O, Boser B et al. Handwritten zip code recognition with multilayer networks. IEEE 1990;2:35-40.*
17 *Hui TW, Tang X, Loy CC. LiteFlowNet: A Lightweight Convolutional Neural Network for Optical Flow Estimation. IEEE 2021;43:2555-9.*
18 *Cai S, Liang J, Gao Q et al. Particle Image Velocimetry Based on a Deep Learning Motion Estimator. IEEE 2020;69:3538-54.*
19 *Shan T, Tay Fr, Gu L. Application of artificial intelligence in dentistry. J Dent Res 2021;100:232-44.*
20 *Orhan K. Bayrakdar I.S. Ezhov M. et al. Evaluation of artificial intelligence for detecting periapical pathosis on cone-beam computed tomography scans. Int Endod J 2020;53:680-9.*
21 *Zheng Z. Yan H. Setzer F.C. et al.Anatomically constrained deep learning for automating dental CBCT segmentation and lesion detection. IEEE Trans Autom Sci Eng 2021;18:603-14.*
22 *Hiraiwa T. Ariji Y. Fukuda M. et al. A deep-learning artificial intelligence system for assessment of root morphology of the mandibular first molar on panoramic radiography. Dentomaxillofac Radiol 2019;48:1-7.*
23 *Aminoshariae A, Kullid J, Nagendrababu V. Artificial Intelligence in Endodontics: Current Applications and Future Directions. J Endod 2021;47:1352-7.*
24 *Murphy M, Killen C, Burnham R et al. Artificial intelligence accurately identifies total hip arthroplasty implants: a tool for revision surgery. Hip Int. 2021 Jan 8; ([Epub ahead of print]) https://doi.org/10.1177/1120700020987526.*
25 *Butler DJ, Wulff J, Stanlet GB, Black MJ. A naturalistic open source movie for optical flow evaluation. Proceedings of European Conference on Computer Vision, Part IV, (2012); pp. 611-625.*
26 *Geiger A, Lenz P, Stiller C, Urtasun R. Vision meets Robotics: The KITTI Dataset. Int J Robot Research 2013;32:1231-7.*
27 *Thomson WT. Theory of Vibration with Applications. 4th edn New Jersey, Prentice Hall, 1972.*
28 *Ahmad M, Pitt Ford TJ, Crum LA. Ultrasonic debridement of root canals: acoustic streaming and its possible role. J Endod 1987;13:490-9.*
29 *Kuah HG, Lui JN, Tseng PSK, Chen NN. The effect of EDTA with and without ultrasonics on removal of the smear layer. J Endod 2009;35:393-6.*
30 *Chopra S, Murray PE, Namerow KN. A scanning electron microscopic evaluation of the effectiveness of the F-file versus ultrasonic activation of a K-file to remove smear layer. J Endod 2008;34:1243-5.*
31 *Mir M, Gutknecht N, Poprawe R, Vanweersch L, Lampert F. Visualising the procedures in the influence of water on the ablation of dental hard tissue with erbium : yttrium-aluminium-garnet and erbium,chromium: yttrium-scandium-gallium-garnet laser pulses. Lasers Med Sci 2009;24:365–74.*
32 *Octavianus F. Visual-based Fluid Motion Estimator with Deep Learning (Magister Thesis) (2021). Bandung, Indonesia: Institut Teknologi Bandung.*